532.542:532.55

Paper No. 147-10

Hydraulic Losses and Flow Patterns in Pipes with Two Bends Combined * (Effects of bend curvature and wall roughness)

By Mitsukiyo MURAKAMI** and Yukimaru SHIMIZU***

In the past, several papers on hydraulic losses and secondary flow in various combinations of commercial elbows have been published, but the effects of the radius of curvature and surface roughness on the flow patterns and hydraulic losses remain unsolved.

In the present paper, by use of four sets of pipe bends having different radii of curvature, the effects of curvature and surface roughness were studied.

1. Introduction

A pipe line in practical use has often many bend portions located close to one another and the losses of the bend are affected strongly by their relative positions. In this case the bend losses are not equal to the sum of each loss which would be experienced if the bend were located separately in a pipe line. This will be due to the mutual interference of the bends on the flow.

Several studies[1]~[4] on this subject have been made in the past, but most of them are related to special combinations of the bends with prescribed bend radii and surface roughnesses.

By using bends of different curvatures and wall roughnesses, hydraulic losses and flow patterns in pipe lines with two bends in various configurations were measured and the effects of bend curvature and roughness of wall were discussed in this paper.

2. Nomenclature

d : diameter of pipe
ΔE_N: difference in total energy flow rates between the entrance and the exit sections of a bend (subscript N:order of bends in a pipe line, N=1 corresponds to the first bend and N=2 to the second bend)
E_{iN}: total energy flow rate at the entrance section of a bend (L_u=0)
E_{oN}: total energy flow rate at the exit of a bend (L_d=0)
ΔH_N: difference in total head losses between the entrance and the exit sections of a bend
L_u : distance of upstream pressure tap from the entrance section of a bend
L_{m1}: length of the spacer between the first and the second bends
L_d : distance of downstream pressure tap from the exit section of a bend
L : total gauge length, $L_u + L_{m1} + L_d$ (Fig.1)
M' : dimensionless expression of angular momentum flux, Eq.(5)
p_1 : static pressure at section 1 located upstream from the entrance section of a bend (Fig.1)
p_2 : static pressure at section 2 located downstream from the exit section of a bend (Fig.1)
p : static pressure at radial distance r
$\bar{p}$: mean pressure at a section
Q : volume flow rate
r_o : pipe radius , =d/2
r : radial distance
R : radius of curvature (Fig.2)
Re: Reynolds number , $=V_m d/\nu$
v_z : axial component of velocity
v_z' : dimensionless axial velocity, v_z/V_m
v_ϕ : tangential component of velocity
v_ϕ' : dimensionless tangential velocity, v_ϕ/V_m
V_m : mean velocity calculated from orifice readings
α_{iN} : kinetic energy correction factor at the entrance section of a bend (L_u=0), Eq.(2b)
α_{oN} : kinetic energy correction factor at the exit section of a bend (L_d=0), Eq.(2b)
γ : specific weight of water
ε : height of surface roughness element
ε/d : relative roughness
θ_o : total angle of a bend (Fig.2)
θ : angular distance of a section in a bend measured from the entrance of the bend
λ : friction factor for a straight pipe
λ_c : friction factor for a bend
ν : kinematic viscosity
ξ : coefficient of bend loss defined by Eq.(4)
ζ_n : coefficient of total bend loss defined by Eq.(1) (subscript n in ζ expresses the number of bends)
ψ : angle of pipe line (Fig.1)

3. Experimental apparatus and procedure

The general arrangement of the test apparatus is shown in Fig.1. To obtain a fully developed velocity profile in the

* Received 10th February, 1972.
** Professor, Faculty of Engineering, Nagoya University, Nagoya, Japan.
*** Assistant Professor, Faculty of Engineering, Mie University.

upstream measuring section, the inlet length before the measuring section 1 was taken sufficiently long and the section was located also at a distance L_u=5d upstream from the first bend. The measuring section 2 was located at a distance of L_d=300d, downstream from the second, and in this section the effect of bends could not be observed. The wall pressures p_1 and p_2 were measured at these two sections L_u=5d and L_d= 300d, respectively. The test pipes had a hydraulically smooth surface and the inside diameter d was 53.8mm.

In Fig.1 ψ and L_{mi} express an angle of twist of pipe line and the distance between two bends, namely, the spacer length, respectively. The values of ψ were changed stepwise 0°,45°,90°,135° and 180°, and the values of L_{mi}/d also changed 0, 1, 2.5, 3.5 and 5.0, respectively.

The bends employed in the experiment had an angle of turn θ_o=90°, and when two bends were combined as in a state of ψ=0° and L_{mi}=0, a bend with the angle doubled, namely, θ_o=180° could be obtained. Flow patterns and pressure distributions within the bends were measured by use of a cylindrical pitot tube: the directions of the measured sections were, θ_o=45°,90°,135°and 180°, respectively, as shown in Fig.2.

To investigate the effects of wall roughness, special bends of brass casting were employed and the bend losses were measured firstly, and then the inside surfaces of the bends were machined carefully to get a hydraulically smooth surface. After these measurements, the inside surfaces of the bends were roughened artificially by sea sands and the tests were repeated. The relative roughness of the bends is given in Table 1. For reference, screw type elbows (JIS) in the Table were also employed in the experiments.

To check the uniformity of velocity distributions in the sections within the bends, a cylindrical Pitot tube with three holes (tube diameter =3.025mm, hole diameter =0.3mm) was traversed along the diameters of N,P,NP and PN, respectively, (Fig. 2).

4. Equation to predict experimental results

With measured pressures of p_1 and p_2, the coefficient ζ_n for the bend loss experienced in the test length can be calculated by the following relation :

$$H = (p_1 - p_2)/\gamma = \lambda(L/d)(V_m^2/2g) + \zeta_n(V_m^2/2g) \quad (1)$$

Evidently, the bend loss is composed of

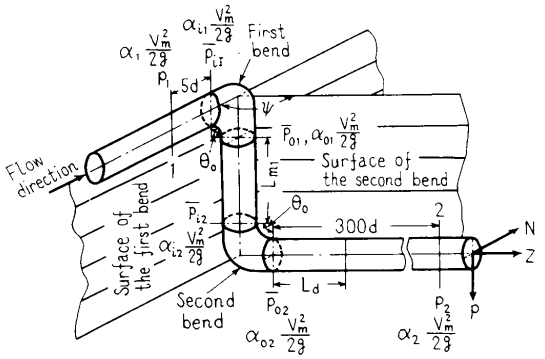

Fig. 1 Definition of pipe bends

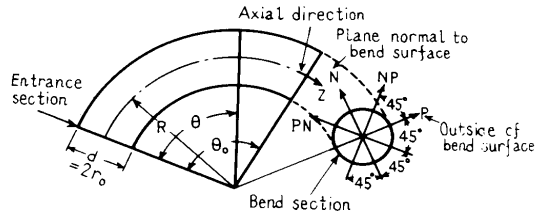

Fig. 2 Definition of bend angle(θ) and directions in bend sections (P,NP, N,PN)

two losses; the one is the internal loss, namely, the loss experienced within the bends and the other is an excess one due to uneven flow components within the downstream straight pipe caused by the bend elements. The total energy flux across a pipe section is calculated by

$$E = \gamma\int_A (p/\gamma + (v_\phi^2 + v_z^2)/2g)v_z dA$$
$$= (\bar{p}/\gamma)\times\gamma Q + \alpha\times\gamma Q\times(V_m^2/2g) \quad (2)$$

where

$$\bar{p} = (\gamma\int_A (p/\gamma)v_z\, dA)/Q \quad (2a)$$

$$\alpha = (\int_A ((v_\phi^2 + v_z^2)/2g)v_z\, dA)/(Q(V_m^2/2g)) \quad (2b)$$

A = sectional area of pipe

With the energy fluxes across the inlet and outlet sections, E_{iN} and E_{oN}, the internal bend loss is given by

$$\Delta E_N = E_{iN} - E_{oN} \quad (3)$$

from which

$$\Delta H_N = (\Delta E_N/\gamma Q) = (\bar{p}_{iN} - \bar{p}_{oN})/\gamma + (\alpha_{iN} - \alpha_{oN})(V_m^2/2g) \quad (4)$$

If the friction loss in the bend is expressed by $\lambda_c(\ell_c/d)(V_m^2/2g)$ (ℓ_c : length of the center line of a bend), then, ΔH_N can be written down as follows ;

$$\Delta H_N = \lambda_c(\ell_c/d)(V_m^2/2g) + \xi(V_m^2/2g) \quad (4')$$

where $\xi(V_m^2/2g)$ will denote a loss caused

Kinds of bends	Bend									Elbow
Kinds of wall surfaces	cast brass bend	cast brass bend	cast brass bend	cast brass bend	fine machined bend	sand rough-ness(1)	sand rough-ness(2)	sand rough-ness(3)	sand rough-ness(4)	JIS screw type elbow
R / r_o	1.6	3	4	6	3	3	3	3	3	1
ε mm	0.205	0.205	0.205	0.205	0.040	0.275	0.65	0.9	2	0.210
d mm	53.8	53.8	53.8	53.8	53.8	53.8	53.8	53.8	53.8	60
ε / d	0.0038	0.0038	0.0038	0.0038	0.00074	0.0051	0.0121	0.0167	0.0371	0.0035

Table 1 (r_o = d/2)

by secondary flow components and flow separations within the bend.

When a pipe line is turned three-dimensionally by use of two bend elements, a swirling flow is generated downstream of the bends, the strength of which can be calculated by

$$M' = \rho\int_0^{2\pi}\int_0^{R}(v_z\, v_\phi\, r^2 dr\, d\phi)/(\rho V_m^2 R^3)$$
$$= \int_0^{2\pi}\int_0^{1} v_z'\, v_\phi'\, r'^2 dr'\, d\phi \qquad (5)$$

5. Experimental results and discussion

5.1 Bend losses and Reynolds number

Effects of Reynolds number, Re, on the losses of two bends combined in various configurations, ζ_2, are shown in Fig.3, where the loss coefficient of a bend located separately, ζ_1, is also indicated for reference. The range of Reynolds numbers, Re= 1.3×10^4~2×10^5, is adopted from a practical point of view. In the bends of brass casting with unfinished surfaces, ζ_2 decreases firstly as Re increases and reaches a minimum at about Re=4×10^4 and then increases asymptotically to a constant. The value of ζ_2 is substantially constant in the range of Re$\geq10^5$. Tendency of these curves has a strong resemblance to that of the curve expressing the relationship between the friction factors of an industrial steel pipe and Reynolds numbers.

The results of different wall roughnesses ((2) and (4) in Table 1) are also shown for the bend of $R/r_o=3$. It may be concluded from Fig.3 that the rate of changes of the curves ζ_2-Re or ζ_1-Re decreases as the roughnesses of bends increase, and all of the bend loss coefficients can be taken to be constant independently of the Reynolds numbers when Re > 10^5.

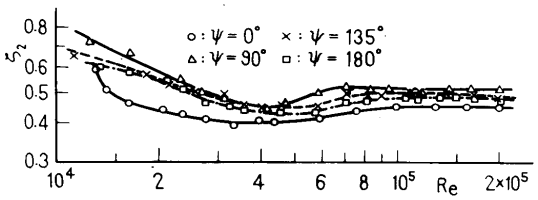

(a) $R/r_o=6$, $L_{m1}=0$, two bends combination (cast brass : $\varepsilon/d=0.0038$)

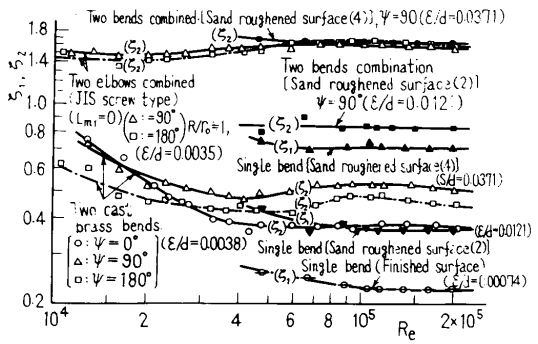

(b) $R/r_o=3$, $L_{m1}=0$ (JIS screw type elbow $R/r_o=1$)

Fig.3 Effects of Reynolds number (Re) on loss coefficient ζ_2 (two bends) (The values of one 90°bend ($R/r_o=3$) and the combination of two JIS screw type elbows are designated on figure (b), too)

5.2 Effects of wall roughness on flow patterns and losses of bends

5.2.1 Bend losses and wall roughness

The relationship between the loss coefficients ζ_1 of a single 90°bend ($R/r_o=3$) and the relative roughness ε/d is shown in Fig.4. When $\varepsilon/d > 0.005$, the roughness effects begin to appear and ζ_1 increases linearly with ε/d. But, when $\varepsilon/d \leq 0.005$, the effects may be negligible and ζ_1 remains substantially constant. In the latter case, the height of the roughness elements ε is approximately equal to or less than that of laminar sublayers on the bend walls. For reference, results of experimental formulae obtained by Pigott[6] (for cast iron bends) and Krüger[7] (for bends of rough surfaces) are also shown in Fig.4, where Pigott's formulae,

$$R/d \leq 1:\ \zeta_1 = 0.157(d/R)^{1.75} + 43.8\,\lambda_c^{1.5}$$
$$R/d > 1:\ \zeta_1 = 0.157(d/R)^{2} + 43.8\,\lambda_c^{1.5} \qquad (6)$$

and Krüger's formulae

$$\zeta_1 = 0.41/\sqrt{R/d} + 0.0175\lambda_c(R/d)\times90° \qquad (7)$$

The results in this experiment can be

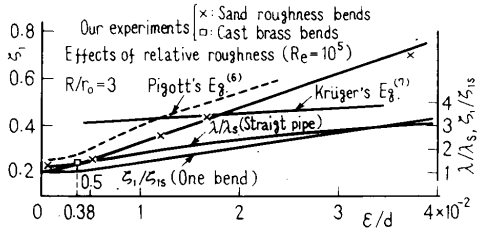

Fig.4 Effects of wall roughness on bend loss coefficient ($R/r_o=3$)

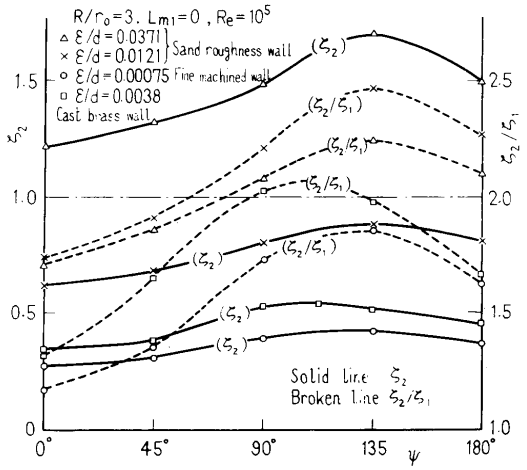

Fig.5 Relation of loss coefficient ζ_2 to relative roughness ε/d

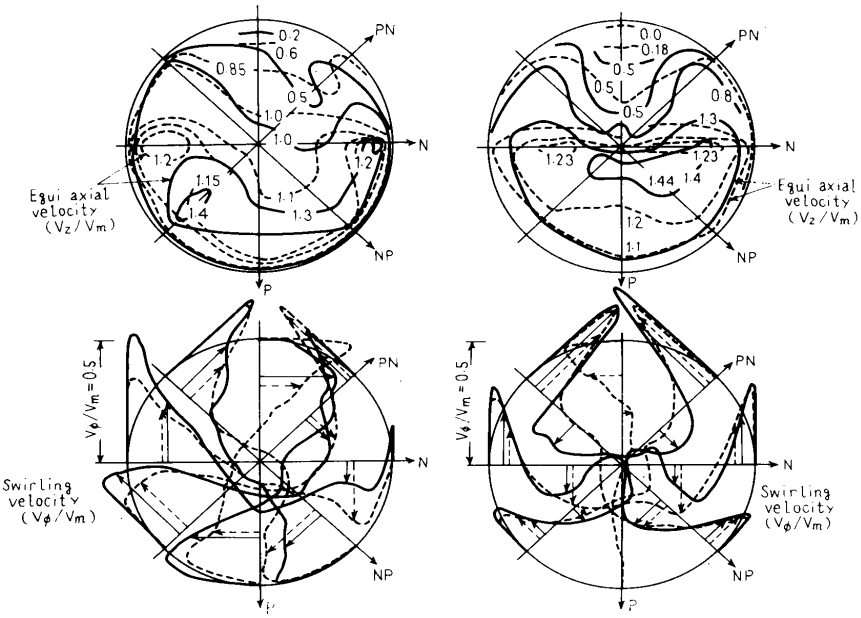

(a) Two bends(ψ=90°, L_{mi}=0) (b) One bend

Fig.6 Relation of velocity distributions at exit of a bend pipe(L_d=0) to relative roughness of wall (R/r_o=3)
solid line: ε/d=0.0371(sand roughness)
broken line: ε/d=0.0121(sand roughness)

expressed approximately by use of Eq.(6). The relative wall roughness of unfinished cast bends lies in the range of $0.0035 \leqq \varepsilon/d \leqq 0.004$ and the roughness effects do not appear on ζ_1. To compare the roughness effects in bend pipes and straight pipes, the values of ζ_1/ζ_{1s} and λ/λ_s are also plotted in Fig.4, where subscript s means a hydraulically smooth surface. The roughness effects on the loss coefficients are more clearly seen in the bend pipe, which will probably be due to an increase of secondary flows and separations in the bends. The relationship between the loss coefficients ζ_2 of two 90°bends combined (R/r_o=3) and the twisted angle ψ is shown as a parameter of the relative roughness in Fig.5. The solid lines express the values of ζ_2 and the broken lines the values of ζ_2/ζ_1. The values of ζ_2 are seen to be changed considerably by ψ. Rate of the change is more accentuated by an increase of ε/d, but the angle ψ at which ζ_2 shows its maximum remains substantially unaltered at $\psi \fallingdotseq 135°$.

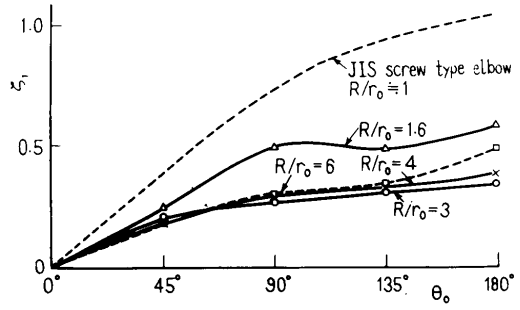

Fig.7 Relation of loss coefficient ζ_1 to bend angle θ_o

5.2.2 Velocity profiles and wall roughness

Figure 6(a) shows velocity distributions at the exit section of the second bend for two kinds of relative roughnesses ε/d =0.0121 (broken lines) and 0.0371 (solid lines), when two bends are combined in a form of ψ=90° and L_{mi}=0. Unevenness of velocity distributions increases as the relative roughness ε/d becomes larger ($V_{\phi max}/V_m$ = 1.4 for ε/d=0.0371 and $V_{\phi max}/V_m$=1.2 for ε/d= 0.0121). Strength of secondary flows measured in that section, M′, also increases with the relative roughness ($M'/2\pi$=0.0703 for ε/d=0.0121 and $M'/2\pi$=0.0754 for ε/d=0.0371). This will probably be due to the fact that an increase of wall roughness brings about much unevennesses of flow velocities in and downstream of the bends and also causes stronger secondary flows. In the bend with more roughened surface(ε/d= 0.0371), Fig.6(b), flow separations are seen to be developed near the inner wall of the bend, but in the bend with less roughened surface (ε/d=0.0121), no separations can be seen. The flow pattern in a JIS screw type elbow has some resemblance to that in the former bend.

5.3 Combination of bends in a pipe line and their losses

5.3.1 U shaped bends

When two bends are composed in a state of ψ=0° and L_{mi}=0, a single U shaped bend can be composed as shown in Fig.2. The loss coefficients ζ_1 for these bends are plotted against the angle of bend θ_o in Fig. 7. The values of ζ_1 increase with θ_o, but different tendencies are seen in either

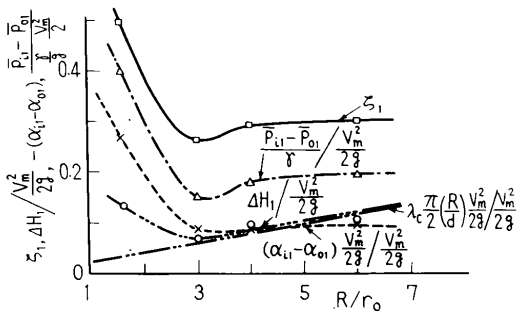

Fig.8 Bend loss between entrance and exit sections of a bend (θ_o=90°)

sides of $\theta_0=90°$, showing more rapid increase in the range $\theta_0<90°$. This phenomenon has a close relationship with the secondary flow development as described below: if the bend angle θ_0 is less than 90°, the secondary flow in the bend increases toward its outlet, and reaches its maximum when $\theta_0=90°$. When $\theta_0>90°$, the secondary flow after attaining the maximum is decreased downwards asymptotically to a constant (see Fig.13). It is noticed that, in the bend of $R/r_0=1.6$, ζ_1 takes a minimum value at $\theta_0=135°$ and in this case, flow separations developed near the inner wall, resulting from a small bend radius, is suppressed by the secondary flow component. The loss component due to a turned passage within a bend, namely, an internal loss, can be discussed by use of Eqs.(4) and (4'). The internal loss ΔH_i in a bend is plotted against R/r_0 in Fig.8, where differences of the pressure and velocity heads between the entrance and exit sections of the bend, together with the friction loss in a straight pipe having the same length, are also plotted. The internal loss $\Delta H_i/(V_m^2/2g)$ is equal approximately to the straight pipe loss $\lambda\times(\pi(R/d)\times(1/2))(V_m^2/2g)/(V_m^2/2g)$ when $R/r_0>3$. But, when the bend is sharply turned and $R/r_0<3$, the internal loss begins to increase abruptly and departs from the straight pipe loss, which will be attributable to the flow separations within the bend.

5.3.2 Losses in three-dimensional double turns and two-dimensional double turns

The coefficients of bend losses caused by two 90° bends combined in various bend configurations are plotted against R/r_0 in Fig.9, where Ito's results for smooth bends ($R/r_0=3.7$) are also shown. In Fig.9(a), the relative bend loss ζ_2/ζ_1 in the case of $\psi=0°$, which corresponds to the case of $\theta_0=180°$ in Fig.7, is always less than 2. When the spacer length L_{m1} is less than 1d, ζ_2/ζ_1 falls as the bend radius R/r_0 increases from unity. In this case, ζ_2/ζ_1 reaches a minimum at $R/r_0\fallingdotseq1.6$, and again increases with R/r_0. When the spacer length L_{m1} is increased beyond 2.5d, the minimum point shifts from $R/r_0=1.6$ to $R/r_0=4$. If a pipe line is bent three-dimensionally in a state of $\psi=90°$ (Fig.9(b)), and also the spacer length L_{m1} is retained small, a single vortex is generated after the second bend. The strength of this vortex increases as the bend radius R/r_0 becomes smaller. In this state, the total bend loss is significantly affected by this single vortex, especially when $L_{m1}=0$, and ζ_2/ζ_1 takes a minimum at $R/r_0=1$ and it falls monotonously as R/r_0 increases ($\zeta_2/\zeta_1\geqq2$ for $R/r_0\leqq3$). As L_{m1} increases,

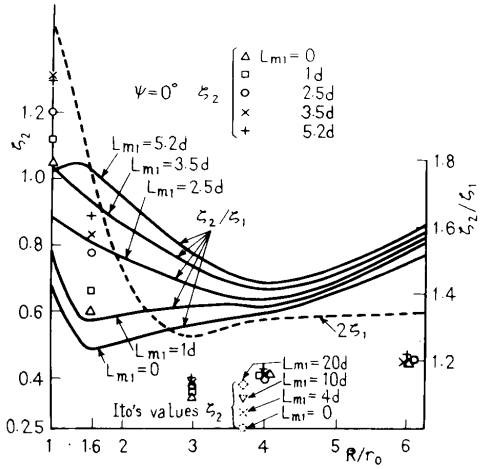

(a) $\psi=0°$, cast brass bends

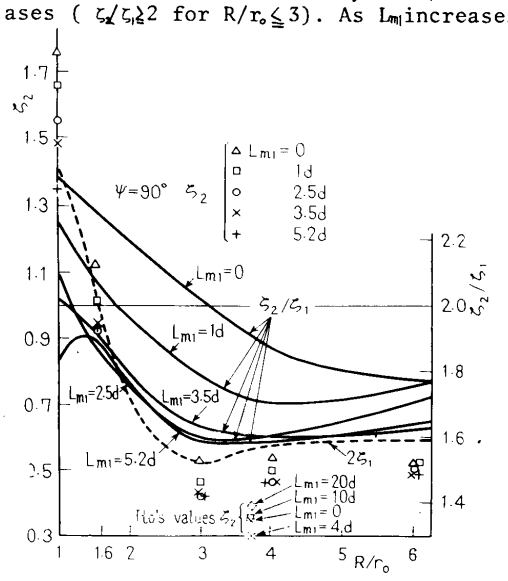

(b) $\psi=90°$, cast brass bends

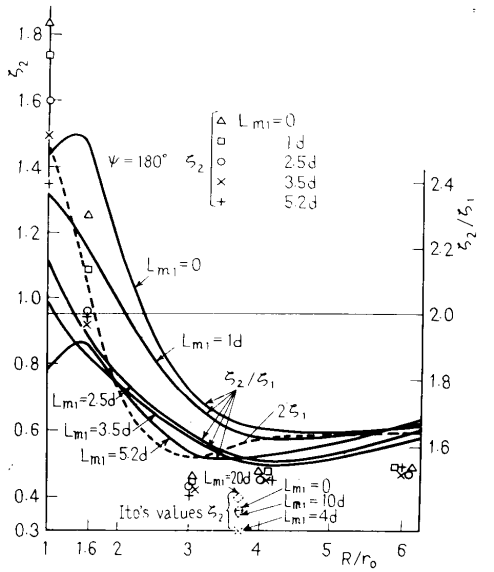

(c) $\psi=180°$, cast brass bends

Fig.9 Relation of loss coefficient ζ_2 to bend curvature R/r_0

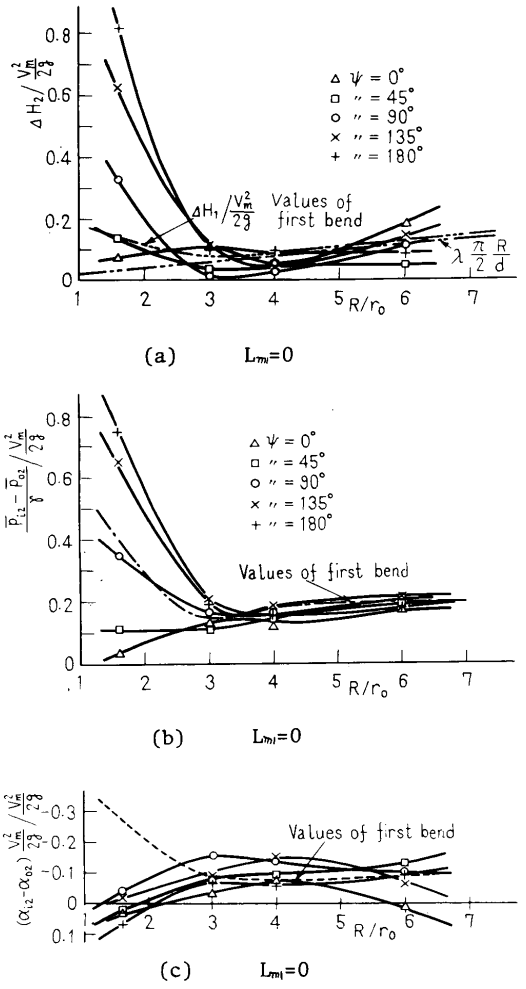

Fig.10 Differences of total energy and pressure and velocity energies between the entrance and exit sections of the second bend

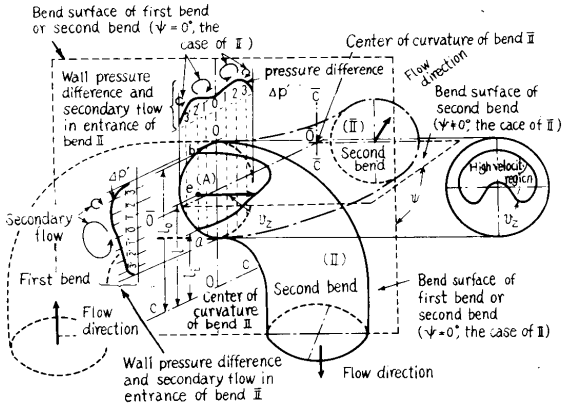

Fig.11 Wall pressure difference and secondary flow in entrance region of second bend
Bend Ⅱ corresponds to ψ= 0°(U bend)
Bend Ⅲ corresponds to ψ≠ 0°(three-dimensional bend)

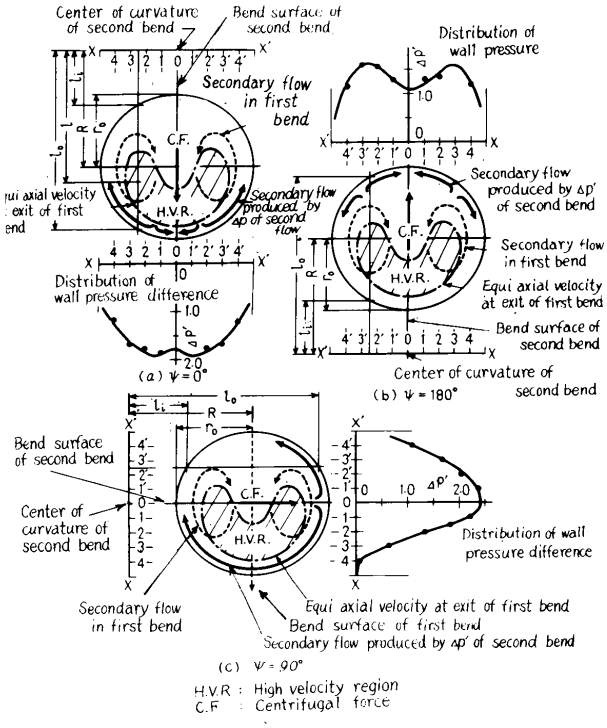

Fig.12 Explanations of the distributions of wall pressure difference and secondary flow in entrance of second bend

the mutual interference of bends is reduced, and the strength of the secondary vortex is weakened. The tendency of curves ζ_2/ζ_1 in this case becomes similar to that observed in $\psi=0°$, and the minimum points of ζ_2/ζ_1 shifts also to the range of $R/r_o=3\sim4$. When the pipe line is bent two-dimensionally in an S shape, i.e., $\psi=180°$ (Fig.9(c)), ζ_2/ζ_1 increases beyond 2, in the ranges of $L_{m1}<1d$ and $R/r_o<2.7$, and ζ_2/ζ_1 decreases below 2, in the range of $L_{m1}>2.5d$. Thus, it may be concluded that the values of ζ_2/ζ_1 will be governed in a complicated manner by L_{m1}, R/r_o and ψ, and by their combinations. It may be noted that, only when $R/r_o<3$ and $L_{m1}<2.5d$, the mutual interference of bends on flows is appreciable and the losses and flow patterns in the bends are greatly affected by the bend combinations. The secondary flows in the bend combinations have a close relationship to the loss coefficient ratio, ζ_1/ζ_1, the details of which will be explained in the following section. A relationship of the internal loss in the second bend ΔH_2 (Eq.(4')) to the bend radius R/r_o for various combinations of bends is plotted in Fig.10(a), where the internal loss in the first bend ΔH_1 is also plotted. When $R/r_o=1.6$, the value of ΔH_2 is governed strongly by ψ, and it exceeds that of ΔH_2 in the range of $\psi\geq45°$. When $R/r_o>3$, ΔH_2 can be assumed to be equal approximately to ΔH_1. Difference of pressure heads between the entrance and exit sections of the second bend is plotted against R/r_o in Fig.10(b). The values of the difference are strongly

affected by ψ in the same way as in Fig.10 (a), when R/r_o is small. Figure 10(c) exibits the difference of velocity heads between the entrance and exit of the second bend. As is seen in the figure, the difference tends to zero when $R/r_o=1.6$, which means that the velocity profiles in these two sections are substantially the same.

5.4 Wall pressures in bends and secondary flow

5.4.1 Change of wall pressures due to the bends of ducts

When fluid particles move on curved paths in a bend, centrifugal forces act on the particles and pressures on the outside wall are elevated over those on the inside wall. This pressure difference calls forth a secondary flow in the bend and deforms the velocity profiles of the primary flow. The deformed primary flow again modifies the secondary flow patterns. These phenomena will be repeated continuously in the bend and the flow pattern changes downward its form in the course of flow.

An explanation on the secondary flows in the second bend which is connected close to the first bend is given in Fig.11. Axial velocity distribution on the exit section of the first bend is shown by (A) in Fig.11. If the second bend is connected to the first one in a direction ((II), $\psi=0°$) as shown in this figure, the curved passage near the inlet of the second bend will bring about a difference in wall pressure between points a and b on the inner and outer walls, and its dimensionless expression is given by

$$\Delta p' = \Delta p / \rho (V_m^2/r) = \int_{\ell_i'}^{\ell_o'} (v_z'^2/\ell') \, d\ell' \qquad (8)$$

where v_z' is an axial velocity at any point on a line a-b, and $\ell' = \ell / r_o$. The calculated values are shown in the upper side of (A) in Fig.11. From this result, the secondary flows designated by the arrowed solid lines are expected to occur. If the second bend is located at another position II ($\psi \neq 0°$), as shown in Fig.11, the distribution of pressure differences takes a quite different pattern from one in the former connection, resulting in some different secondary flows. It follows that the secondary flows which would be expected in the inlet region of the second bend may be decided by relative positions of the two bends. Figures 12(a),(b) and (c) show the distribution of difference pressures and the secondary flows for the angles of two bends, $\psi=0°$,180° and 90°, respectively, ($R/r_o=1.6$ and $\theta_o=90°$). The chain lines in each section express equi-axial velocity curves observed at the exit section of the first bend or the inlet section of the second bend.

When $\psi=0°$ and 180°, curves of $\Delta p'$ are

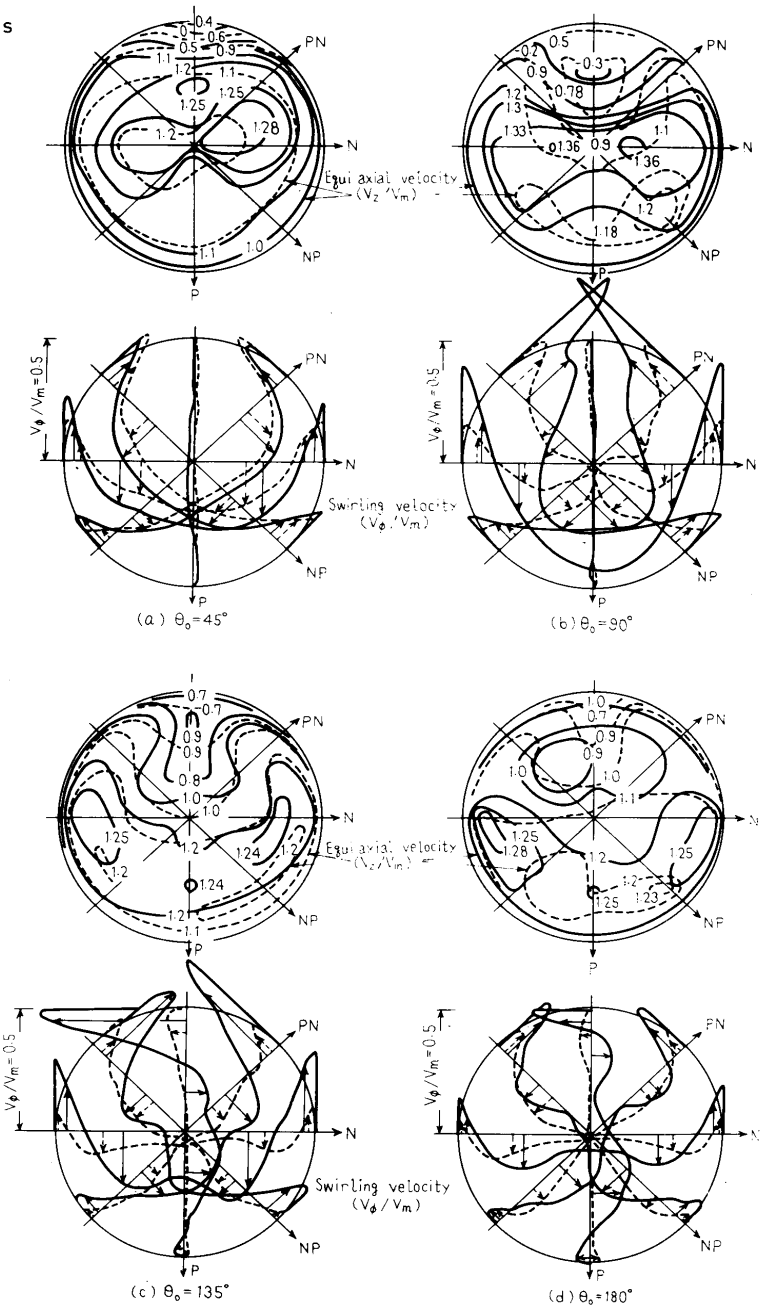

Fig.13 Velocity distributions at exit of U bend($L_d=0$)
(a) $\theta_o=45°$, (b) $\theta_o=90°$, (c) $\theta_o=135°$, (d) $\theta_o=180°$
solid line: $R/r_o=1.6$, broken line: $R/r_o=6$
(cast brass bend)

almost symmetric with respect to the bend plane o-o, but when ψ= 90° the curve becomes asymmetric.

5.4.2 Deformation of velocity profiles due to bends

(1) Two-dimensional turns: U shaped bends (ψ=0°, L_{mi}=0)

Distributions of main(axial) and secondary(tangential) components of velocities at the sections of angular positions θ_o= 45°,90°,135° and 180° are given in Fig.13, where the solid and broken lines denote the results for R/r_o =1.6 and 6, respectively. The secondary flow(v_ϕ/V_m) is seen to be intensified as the bend angle θ_o increases from 45° to 90°, but it is weakened by an increase of θ_o within the range of θ_o>90° , which can be explained from the results shown in Fig.12(a). When two bends having a same bend angle of θ_o=90° are connected in a state of ψ=0° and L_{mi}=0 as shown in Fig.12(a), these result in a single bend with an angle of θ_o=180°(90°×2), and $\Delta p'$ shown in Fig.12(a) will correspond to the difference pressure at the section situated in the middle of the 180°bend. In this section, a pair of small vortices having a counter sense to the main vortices is seen to be generated as is already explained , and the newly generated vortices act to reduce the main vortices. The counter vortices grow more in the downstream region and hence, the secondary flow which will be observed in the bend also diminishes.

The region of high velocity(axial component) is in the inner portion of the bend in the case of θ_o=45° ,but the region shifts to an outer portion as θ_o increases (Fig.13). The shifting phenomenon is related closely to the secondary flow development in the bend.

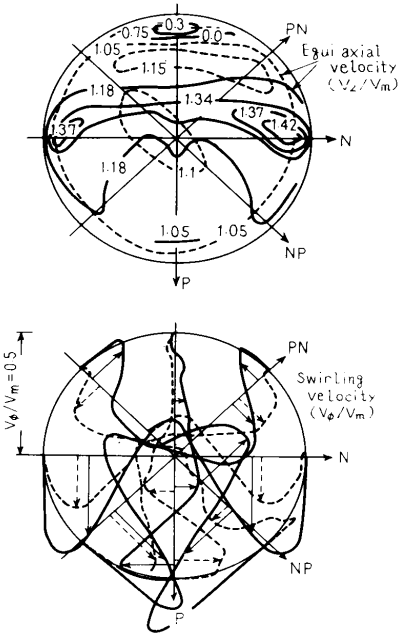

Fig.14 Velocity distribution at the exit of S shaped bends(L_d=0) (two 90°bends, ψ=180°,L_{mi}=0, cast brass bends), solid line:R/r_o =1.6, broken line:R/r_o =6

(2) Two-dimensional turns: S shaped bends(ψ=180°, L_{mi}=0)

Figure 14 shows velocity distributions at the exit section of a second bend in S shaped turn(ψ=180°, L_{mi}=0). The distribution of $\Delta p'$ just after the inlet section of the second bend is shown in Fig.12(b), in which a depression of $\Delta p'$ is seen in the central plane o-o. Thus, the secondary flow created already in the first bend will be strengthened by this distribution of difference pressures $\Delta p'$, and the resulting secondary flow tends to uniformarize vigorously the axial velocities in the bend . The uniformity in case of R/r_o =1.6 is less attainable than in case of R/r_o =6, because of flow separations near the inner wall.

(3) Three-dimensional turns: twisted S shaped bends

When two bends are combined in a shape of ψ=90° and L_{mi}=0, the curves of $\Delta p'$ just after the entrance of the second bend take an asymmetric shape against the line o-o(locus of the bend plane) as shown in Fig.12(c). The shape of the curves is changed continuously towards the outlet of the bend in the course of flow. Some examples are shown in Fig.15, where the measured sections of $\Delta p'$ in the second bend are taken to be θ=45°,90°,135° and 180°, respectively. As an example, let us observe the results for the case R/r_o =3.

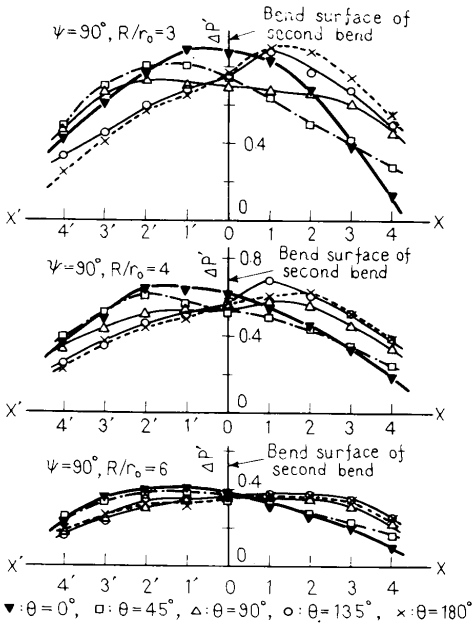

▼:θ=0°, □:θ=45°, △:θ=90°, ○:θ=135°, ×:θ=180°

Fig.15 Change of the distributions of wall pressure difference along the bend center

The distribution curve of $\Delta p'$ at the section $\theta=45°$ (marked by symbol □) has peak in the left hand side of the origin o, and that of $\Delta p'$ at the section $\theta=135°$ (marked by simbol ○) in the right hand side of o, and the two curves are nearly symmetric with respect to the ordinate axis. Hence, secondary flows driven by this distribution of differences $\Delta p'$ change the signs. Alternate changes of these flow patterns are repeated continuously till the exit end of the bend, the details of which will be described in another paper[8].

6. Conclusions

A pipe line was bent in various configurations with two right angled bends, and effects of bend radius and wall roughness on flow patterns and hydraulic losses were examined experimentally. The results can be summarized as follows.

(1) The bend loss is almost unaffected by Reynolds numbers in the range of $Re \geq 10^5$.

(2) The value of R/r_o has a decisive effect on the bend loss (Fig.9). With $R/r_o \leq 1.6$, flow separations occur near the inner wall of bends and affect the flow patterns and the losses in the bends. With $R/r_o > 3$, the flow separations are almost avoid and the bend loss is caused mainly by skin friction and secondary flows due to the bend.

(3) Effects of wall roughness on hydraulic loss appear more appreciably in bends than in straight pipes, which will be attributable to an increase of secondary flow due to roughness elements in bends.

(4) In a U shaped combination of bends having a total bend angle of $\theta_b > 90°$, secondary flows caused by the bend passage grow progressively toward downstream till they reach some maxima at the section of $\theta=90°$, after which the secondary flows decrease asymptotically to a certain value.

(5) In an S shaped combination of bends (two-dimensional turn), secondary flows created in the first bend are intensified in the second one, when the distance between the two bends L_m is sufficiently short.

(6) In a twisted shaped combination of bends (three-dimensional turn), flow patterns, including secondary flows, change alternately along the bend center line, if the line is sufficiently long.

References

(1) Murakami,M. et.al.,Bull.JSME,Vol.12, No.54(1969-12),p.1369.
(2) Murakami,M. and Shimizu,Y.,Bull.JSME, Vol.16,No.96(1973-6),p.981.
(3) Murakami,M. and Shimizu,Y.,Trans.Japan Soc.Mech.Engr.(in Japanese),Vol.40 ,No.334(1975-6),p.1739.
(4) Ito,H.,Mem.Inst.High Speed Mech.,Tohoku Univ.,(in Japanese),Vol.15,No.142 (1960/1961),p.37.
(5) Ito,H.,Trans.ASME,Ser.D,82(1960-3),p. 131.
(6) Pigott,R.J.S.,Trans.ASME,Vol.79,No.8 (1957-11),p.1767.
(7) Krüger,H.,Maschinenbau Technik,Vol.19 ,No.3(1970),p.147.
(8) Murakami,M. and Shimizu,Y.,Trans.Japan Soc.Mech.Engr.(in Japanese),Vol.43 ,No.375(1977-11)